Sánchez-Escuderos, D.; Ruiz-Garnica, J.; Baquero Escudero, M.; Soto Pacheco, P.; Boria Esbert, VE.; Tosso, G.; Angeletti, P.... (2019). Evanescent-Mode Ridge-Waveguide Radiating Filters for Space Applications. IEEE Transactions on Antennas and Propagation. 67(10):6286-6297. https://doi.org/10.1109/TAP.2019.2920272

Evanescent-Mode Ridge-Waveguide Radiating Filters for Space Applications

Daniel Sánchez-Escuderos, *Member, IEEE,* Jesús Ruiz-Garnica, Mariano Baquero-Escudero, *Member, IEEE,* Pablo Soto, *Member, IEEE,* Vicente E. Boria, *Fellow, IEEE,* Giovanni Toso, *Senior Member, IEEE,* Piero Angeletti, *Senior Member, IEEE,* Marco Guglielmi, *Fellow, IEEE*

***Abstract*—This paper describes a new family of all-metallic radiators based on below-cutoff apertures fed by evanescent-mode ridge waveguide filters. The pass band of the filters and the polarization of the apertures are configured to radiate orthogonal signals at different center frequencies. The simultaneous operation of these radiators in an array configuration results in interleaved apertures producing overlapped fields. This strategy reduces the volume and weight of the antenna system, which is a specially appealing characteristic in satellite antennas. Each isolated evanescent-mode filter ends in a small-size aperture and is designed following a novel synthesis procedure. Next, the radiating elements are combined, and the resulting array is analyzed as a multiplexer from the input ports to the free-space region thus accounting for all mutual couplings between different apertures. To validate the theoretical formulations, a prototype has also been manufactured. The results obtained show very good agreement between simulation and measurements in terms of reflection coefficient, side-lobe level and realized gain, thereby fully validating the new family of radiating arrays.**

***Index Terms*—Below cutoff apertures, Evanescent-mode ridge-waveguide filters, Multiple spot-beam antennas, Overlapped arrays, Satellite communications.**

I. Introduction

HIGH throughput satellite (HTS) systems allow broadband two-way communications for fixed or mobile users, such as aircraft, high-speed trains or emergency vehicles. The implementation of these systems in the Ka band [1], [2] can provide a capacity of several hundreds of Gbits/s by means of Multi-Beam Antennas (MBA) with frequency and polarization reuse. Typically, two frequencies and two polarizations are used (4 colors).

The most mature MBA architecture is based on 3-4 main reflectors in a Single-Feed-per-Beam (SFPB) configuration. This solution permits to minimize spillover and to generate a continuous coverage of high-gain spotbeams with the required beam-to-beam isolation [3], [4]. The total efficiency of the system is maximized by using large-aperture high-efficiency feeds [5]. Main drawback is related to the number of main reflectors, difficult to accommodate onboard a satellite.

Solutions based on Multiple Feed per Beam (MFPB) architectures have been proposed with the objective of reducing the number of main reflectors [6]. These solutions overlap the footprints of the beams on the focal plane of the reflector to generate all the beams with only one main reflector (possibly two for uplink and downlink). In [7]–[9], for instance, overlapped beams are generated by arrays of circular apertures operating simultaneously for two different colors. In [10], [11] the beams are produced by adding a Fabry-Perot cavity in front of an array of feeds. These solutions, however, are rather complex and have been implemented only for a limited number of beams.

Alternatively, Direct Radiating Arrays (DRAs) have been proposed as a flexible solution for multiple spot-beam applications [12]. These arrays, where all the elements participate to the generation of all the beams, must be fed by sophisticated Beam-Forming Networks (BFNs) which tend to be expensive and lossy. A strategy to minimize complexity and losses consists of using overlapped sub-arrays with all-metallic BFN and a plurality of amplifiers inserted at optimal locations [13]. Furthermore, the use of aperiodic arrays has also been proposed to reduce the number of elements and the cost of the antenna, while producing, at the same time, low grating lobe levels [14]–[16].

DRAs have become a promising solution, not only for satellite communications but also for radar applications. The specific choice of the radiating elements, however, is still an area of open research. In multi-frequency/dual-polarization antennas, the radiating element should be capable of covering all the required bands/polarizations. In alternative, if radiating elements operating individually at single frequency/polarization are used, they must be interleaved in a small periodic cell. Recently, fully-overlapped sub-arrays working in several bands (X, Ku and Ka) have been proposed in [17], [18]. However, the use of several dielectric layers restricts their range of applicability.

In this paper, we propose a new all-metallic radiating element formed by four apertures radiating two different frequencies and two different polarizations (four colors) [19]. The radiating elements are four square apertures $(0.34\lambda_0 \times 0.34\lambda_0)$ in a 2×2 arrangement.

Other implementations of this type of radiating elements have been proposed in the past using Substrate Integrated Waveguide (SIW) [20], [21], Low-Temperature Cofired Ce-

This work was supported by the Spanish Ministry of Economics and competitiveness under projects TEC2016-79700-C2-1-R, TEC2016-78028-C3-3-P, TEC2013-47037-C5-1-R and TEC2016-75934-C4-1-R

D. Sánchez-Escuderos, Jesús Ruiz-Garnica, M. Baquero-Escudero, P. Soto, V. E. Boria and M. Guglielmi are with the Instituto de Telecomunicaciones y Aplicaciones Multimedia (ITEAM) of the Universitat Politècnica de València, c/ Cami de Vera s/n, 46022 Valencia, Spain (e-mail: dasanes1@iteam.upv.es, jrgarnica@iteam.upv.es, mbaquero@dcom.upv.es, pabsopac@dcom.upv.es, vboria@dcom.upv.es, marco.guglielmi@iteam.upv.es).

G. Toso, and P. Angeletti are with the European Space Agency, 2200 AG Noordwijk, The Netherlands (e-mail: giovanni.toso@esa.int, piero.angeletti@esa.int).

ramic (LTCC) [22], microstrip [23], [24], and metallic waveguide [25] technologies with quite good results. However, the major problem in using conventional waveguide technology is the restriction to use apertures with a cross section that is greater or equal to the cross section of the feeding (above cutoff) waveguide. In [25], for instance, the lateral size of the housing and the apertures are $0.7\lambda_0$. This choice avoids grating lobes, but makes it impossible to implement interleaved apertures with different frequencies/polarizations. A size reduction leads to the use of below-cutoff apertures, which cannot be directly fed by waveguide sections of the same or smaller dimensions due to the high attenuation that guided waves suffer below cutoff.

The novelty of the solution proposed in this work is the use of waveguide apertures with a side of about $0.35\lambda_0$, so that apertures of the same color can be separated less than $0.8\lambda_0$ in the interleaved sub-arrays. As a result, DRAs in hollow waveguide technology with four different colors, and without grating lobes, become possible. Although the resulting square apertures are below-cutoff, their proper feeding is achieved with the integration of the radiating aperture with an evanescent-mode filter. This solution provides, in addition, the filtering functionality required to isolate the signals corresponding to different frequency bands, and minimizes the effects of passive intermodulation (PIM) in the system.

The use of small aperture antennas based on evanescent-mode filters was already proposed in [26], where an aperture of size $0.46\lambda_0 \times 0.23\lambda_0$ integrated in a ridge waveguide band-pass filter was described. Only a single antenna was considered in [26], which was designed to provide the highest bandwidth (at the expense of selectivity and band-pass return loss performance). In this work, however, a more complex cell composed of 2×2 below-cutoff apertures has been conceived. Moreover, the evanescent-mode band-pass filters have been designed to fit the bandwidth of each frequency band, thus separating in an optimal way the different colors used in the cell. In this context, a novel procedure for general filtering aperture antennas has been developed. The novel procedure is able to implement the prescribed transfer function reducing (or possibly avoiding) the final electromagnetic (EM) optimization.

After the individual design, each small size evanescent-mode aperture antenna is combined in a novel radiator. The design of the radiator has been carried out considering the structure as a four-channel multiplexer, where the free-space plays the equivalent role of the manifold in a filter multiplexer [27]. The full-wave EM analysis is based on a rigorous multimode equivalent network representation for both the feeding filters [28], and the radiating apertures [29], thereby rigorously accounting for all mutual coupling effects.

The paper is organized as follows: first, we evaluate in Section II the performance of an array of interleaved below-cutoff apertures. Next, in Section III, we describe a novel design method for separate evanescent-mode ridge-waveguide filters with one end radiating into the free-space. The results of this design are then used as a starting point in Section IV for the design of the complete four-color radiator. To continue, we show in Section V comparisons between the simulated and measured performance of a radiator prototype manufactured in aluminum. The paper is concluded in Section VI with a summary of the results obtained.

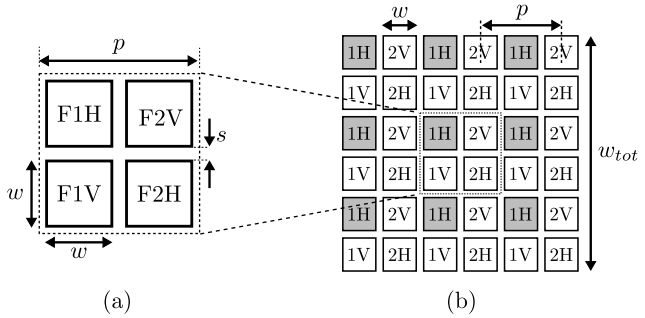

Figure 1. Interleaved subarrays of square apertures: (a) radiating element composed of four square apertures, and (b) four 3×3 interleaved subarrays. The shadowed apertures form a subarray for a single color.

II. Interleaved subarrays of below-cutoff apertures

The proposed all-metallic radiating element is shown in Fig. 1 (a). The structure is composed of four square apertures radiating four different colors (F1V, F2V, F1H, and F2H). Two bands centered at frequencies F1 and F2, and two orthogonal polarization, namely, vertical (V) and horizontal (H). The size of the apertures and their separation are w and s, respectively.

The combination of several radiators of the same type forms an array of apertures composed of four interleaved subarrays with the phase center slightly shifted by the aperture width. Fig. 1 (b) shows an example of four 3×3 interleaved subarrays (the shadowed apertures highlight one of the subarrays). This configuration allows for the overlapping of orthogonal beams in the radiating plane, as required by multiple spot-beam systems.

The design of the radiating element starts with the definition of the size of the apertures. This size must be chosen so that p, namely, the period of the apertures in the subarrays, is kept below 0.8λ to avoid the appearance of higher order grating lobes in the radiation pattern. Considering a separation s of about 0.05λ, namely, 1 mm at 10 GHz, a w smaller than 0.35λ is needed. Consequently, the apertures of the proposed all-metallic radiating element must be below cutoff. Observe that 0.8λ is an upper limit. Apertures can be smaller at the expense of increasing the number of elements to keep the same gain level.

A key issue in using below-cutoff apertures is how to properly feed them. Fig. 2 shows the total efficiency (including radiation and reflection losses) of several square apertures as a function of the length of the feeding waveguide. As can be observed, above cutoff apertures ($w = 0.56\lambda$) produce 100% efficiency for any length, however below-cutoff apertures suffer a remarkable degradation of the efficiency for large feeding lengths (specially for $w = 0.34\lambda$).

The degradation shown in Fig. 2 can be completely avoided, however, if the length of the below-cutoff waveguide and the step to the free-space are used to implement the impedance inverter that is needed at the output port of a waveguide filter.

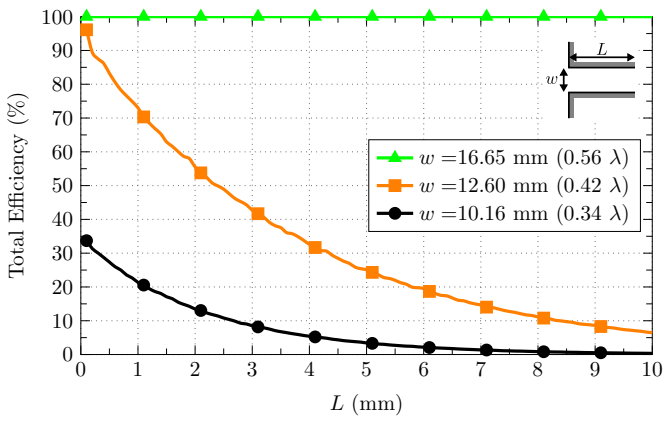

Figure 2. Total efficiency of a square aperture at 10 GHz.

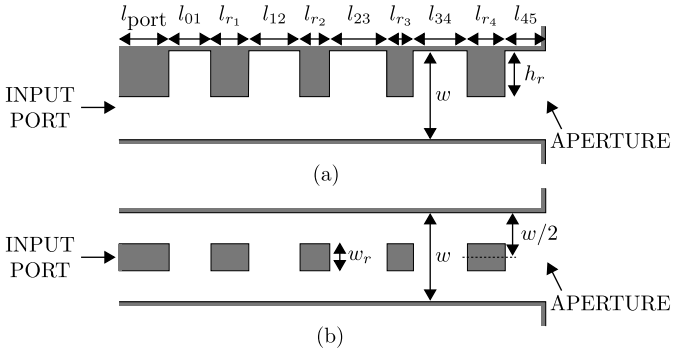

Figure 3. Configuration of a 4-pole evanescent-mode filter ended in a below-cutoff aperture: (a) lateral view and (b) upper view. Resonators are implemented by single-ridge waveguides. The housing and the aperture have square-section of side w.

In this context, therefore, we propose to use evanescent-mode ridge waveguide filters to feed the radiating apertures. The filters are formed by lengths of ridge waveguides, acting as resonators, and lengths of below-cutoff waveguides, acting as inverters. The below-cutoff aperture and the step between the aperture and the free-space is in fact part of the last inverter of the filter, thereby obtaining an efficient feeding, and, at the same time, a more compact structure.

The different frequency bands (F1 and F2) will, therefore, be separated by the transfer function of the filters attached to each below-cutoff aperture. The optimal trade-off between selectivity and filter order results in important benefits in terms of losses, size, weight, cost and tolerance to manufacturing errors. It is important to note that the evanescent-mode filters corresponding to horizontal polarization apertures will be the same used for vertical polarization after performing a 90 degree rotation (to orientate the TE_{10} electric field at the below-cutoff aperture in the horizontal axis). As a result, only two different filters must be designed. In the next section we describe a novel procedure for the design of the filters, with optimal (equiripple) transfer functions.

III. Design of Below-Cutoff Apertures Fed by an Evanescent-Mode Ridge Waveguide Filter

The design of small-aperture evanescent-mode waveguide filtering antennas has been recently considered in the literature [26]. The proposed technique relies on the classic synthesis procedure of evanescent-mode filters [30], that has been extended to include the effect of the complex load provided by a radiating aperture. This method has been conceived to obtain the largest bandwidth, as both the input and output inverters (the ones that are more relevant to control the filter bandwidth) are essentially removed. This fact is illustrated in Fig. 6 of [26], showing how the last ridge is located at the aperture plane. As a result, a wideband and compact filtering antenna is obtained. The method in [26], however, cannot properly control the input/output coupling levels, and therefore does not produce the optimal filter transfer function to the free-space (normally equiripple) which provides the highest selectivity for the specified maximum passband return loss [31].

For the particular application discussed in this paper, this procedure is clearly unsuitable. This is because the filtering antenna bandwidth must fit the given frequency band, the return loss must be kept low (to avoid reflections reducing the power delivered to the apertures), and a transfer function with optimal selectivity must be sought. All the requirements can be met at the same time only if all degrees of freedom provided by the basic filter structure are exploited, including also input and output couplings. The topology under consideration is shown in Fig. 3, where the lengths of the ridge resonators and the below-cutoff waveguide sections between them are used to control the response. In contrast to [26], there is a distance between the last ridge resonator and the aperture to adjust the output coupling. The input port can be a ridge waveguide (as shown in Fig. 3) or can be based on a coaxial excitation. The distance between the input port and the first ridge resonator will be used to adjust the input coupling.

To design the individual filters, we propose in this paper a more modern approach based on the slope parameter, replacing the classic iterative synthesis procedure of evanescent-mode filters detailed in [32]. This novel procedure is general, and can be applied to almost any in-line filter topology. The procedure starts with the basic synthesis equations of the lumped-element bandpass prototype in admittance form for a filter of order n:

$$J_{0,1} = \sqrt{\frac{Y_{\text{inp}}\Delta b_1}{g_0 g_1}} \tag{1a}$$

$$J_{i,i+1} = \Delta\sqrt{\frac{b_i b_{i+1}}{g_i g_{i+1}}} \quad , \quad i = 1, 2, \ldots, n-1 \tag{1b}$$

$$J_{n,n+1} = \sqrt{\frac{\Delta b_n Y_{\text{outp}}}{g_n g_{n+1}}} \tag{1c}$$

where $\Delta = (f_2 - f_1)/f_0$ is the fractional bandwidth of the filter, Y_{inp} and Y_{outp} are the admittances of the input and output ports at the center frequency $f_0 = \sqrt{f_2 f_1}$, respectively, g_i are the normalized coefficients of the chosen transfer function, and b_i denotes the slope parameter of each resonator of the evanescent-mode filter.

The expressions in (1) represent a generalized form of the normalized expressions reported in section II of [25], which

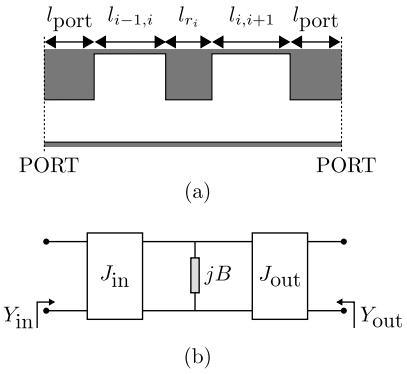

Figure 4. Topology considered for extracting the susceptance of a central resonator of the evanescent-mode filter: (a) Physical structure, and (b) equivalent lumped-element model.

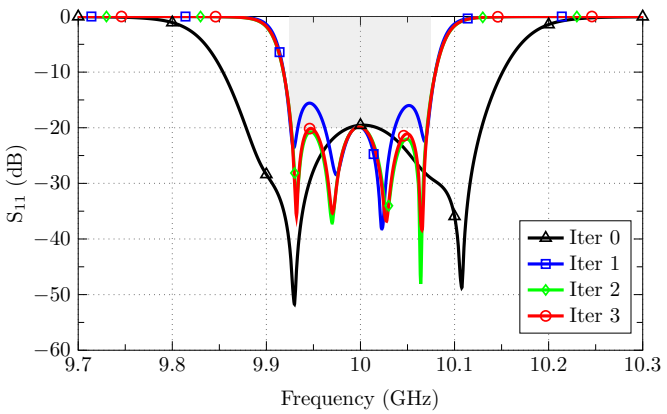

Figure 5. S_{11} parameter of the 4-pole filter designed with the proposed technique for the first four iterations. Shadowed region shows the specifications of the filter.

now allows different slope parameters b_i for each resonator. For an ideal half-wavelength waveguide resonator operating with a TE mode, the slope parameter is theoretically given by:

$$b_{\text{ideal}} = \frac{\pi}{2} Y_0 \left(\frac{\lambda_{\text{g0}}}{\lambda_0} \right)^2 \tag{2}$$

where Y_0, λ_{g0} and λ_0 denote, respectively, the characteristic admittance, guided wavelength and free-space wavelength of the waveguide mode at the filter center frequency f_0.

For a given transfer function shape (i.e., coefficients g_i), these expressions can be used to perform an initial synthesis of the filter. The length of the evanescent mode sections performing the coupling between resonators and input/output ports are first determined in order to obtain the corresponding admittance inverter parameter J computed by (1). Next, the length of each ridge waveguide section is adjusted to obtain the resonance at the center frequency f_0 taking into account the loading effect of its input and output evanescent mode sections. As a result, an initial value of all the filter dimensions is obtained. The simulated response of the resulting filter will be more or less close to the desired one (depending on the particular filter topology), and a full-wave optimization must be carried out to obtain a compliant transfer function. This procedure is the one followed in [25].

The main inaccuracy of this method is that the slope parameter used in (1) is the one of an ideal resonator, and thus, all the resonators with the same cross-section will have the same value. This is, indeed, a rough approximation of the reality, where each ridge resonator has different length and loading conditions. A technique has been proposed to take into account the slope parameter in a more accurate way [33]. In that work, the frequency dependence of each isolated coupling element is extracted and assigned to the slope parameter of its adjacent resonators. In this paper, we move a step further by extracting the slope parameter from the full-wave simulation of the real resonator loaded with its input and output coupling elements as a whole. This approach has the benefits of including also the higher-order mode interactions between all elements, and the effective frequency behavior of the real waveguide resonator. For a central resonator of an evanescent-mode filter, the structure to be simulated is shown in Fig. 4(a). An equivalence between such structure and its corresponding part of a lumped-element prototype (see Fig. 4(b)) is carried out. Then, the simulated input reflection coefficient is equated to the one of the equivalent circuit, obtaining:

$$S_{11} = e^{-2j\theta} \frac{J_{\text{out}}^2 Y_{\text{in}} - J_{\text{in}}^2 Y_{\text{out}} + jBY_{\text{out}}Y_{\text{in}}}{J_{\text{out}}^2 Y_{\text{in}} + J_{\text{in}}^2 Y_{\text{out}} + jBY_{\text{out}}Y_{\text{in}}} \tag{3}$$

where θ takes into account the different position of the reference planes in both circuits (related to l_{port}). Taking the magnitude of the simulated S_{11} parameter in (3), the value of the susceptance B in terms of frequency can be derived. From such term, the slope parameter of the resonator is evaluated according to the classic definition:

$$b = \frac{\omega_0}{2} \left. \frac{dB(\omega)}{d\omega} \right|_{\omega=\omega_0} \tag{4}$$

which, now, has the real variation with frequency of the susceptance of the resonator including also the loading effect of the input and output admittance inverters. Note that the slope parameter will be different for each resonator, thus justifying the use of the generalized expressions compiled in (1) instead of the normalized ones usually employed in filter synthesis procedures [25].

Introducing the new slope parameters into (1), the values of the admittance inverters are updated and a new synthesis of the filter dimensions is carried out. An iterative procedure is then followed, so that, after a very few iterations, excellent filter dimensions are obtained (which, at most, will only require a minor refinement).

The synthesis procedure just described is general, and can therefore be applied for any filtering antenna fed by an in-line direct-coupled cavity filter. In addition, it is also suitable to be included into a Computer-Aided Design (CAD) framework.

In order to illustrate this procedure, the proposed technique has been applied for the design of a small-size aperture fed by a fourth-order evanescent-mode filter with ridge input port (see Fig. 3) and equiripple response. The housing (and aperture) side is $w = 10.16$ mm (about 0.34λ), the height and width of

Table I
DIMENSIONS (in mm) OF THE FILTER OPTIMIZED WITH THE PROPOSED TECHNIQUE FOR THE FIRST 4 ITERATIONS

Parameter	Iter 0	Iter 1	Iter 2	Iter 3
l_{01}	4.5243	6.1251	6.1189	6.1198
l_{r_1}	7.4067	6.7709	6.7726	6.7723
l_{12}	9.9077	12.8890	12.8822	12.8871
l_{r_2}	6.3521	6.2443	6.2444	6.2443
l_{23}	11.1428	14.0870	14.0851	14.0903
l_{r_3}	6.3521	6.2388	6.2439	6.2423
l_{34}	9.9077	13.4875	13.0330	13.0899
l_{r_4}	3.6050	5.2213	4.9902	5.0207
l_{45}	2.1200	4.2776	3.8219	3.8768

the ridges are $h_r = 4.75$ mm and $w_r = 3.5$ mm, respectively. A return loss better than 20 dB is requested in the filter passband, extending from f_1 =9.925 GHz to f_2 =10.075 GHz. The admittance of the output port (i.e, free-space) is taken to be 1/η, where η is the free-space impedance. The response obtained after the initial dimensional synthesis (i.e, the one carried out using the slope parameter (2) for all the ridge resonators) is the one labelled as Iter 0 in Fig. 5, showing a huge bandwidth (more than 70% higher than the specified one) and a somewhat degraded return loss in the bandpass. This is the response that can be obtained with the procedure detailed in [25], which would require substantial optimization to obtain a final filter fulfilling all specifications.

Following the novel procedure described in this paper, the real slope parameter of each resonator taking into account its loading condition can be computed, and the prototype parameters can be readjusted accordingly. As a result, the response is improved iteration after iteration and reaches convergence with only three iterations (see Fig. 5). The evolution of the filter dimensions at each iteration is compiled in Table I. The final response is excellent and does not require a final full-wave EM optimization. The design procedure is therefore concluded.

It is now important to point out the differences between the final response in Fig. 5 and the one obtained in [26] to achieve the widest bandwidth. As it can be seen, an optimal equiripple response with all the reflections zeros of the response placed in the imaginary axis is obtained. It is well known that this response (for in-line topologies without transmission zeros) is the one providing the maximum selectivity for a prescribed filter order, and a given return loss in the passband [31]. For this particular type of applications, involving different frequency bands in the same radiator, it is essential to obtain a good isolation between the different frequency bands to provide the purest signal to each below-cutoff aperture. This will avoid unwanted interference that could reduce the measured performance of the final antenna.

IV. MULTIPLEXER OF BELOW-CUTOFF APERTURES

The technique proposed in the previous section can be used to design evanescent-mode ridge-waveguide filters radiating into free-space. Although the technique is described for a single filter opened to a single aperture in an infinite ground plane, the extension to an arbitrary number of filters and apertures is straightforward. The only additional point consists in taking into account the relative position of the different apertures in the ground plane, as described in [29]. The resulting structure can indeed be seen as a multiplexer from N feeding filters to the free-space region (which acts as the manifold combining the signals in a common port). In addition, since the various radiating apertures radiate in orthogonal polarization, the array implements also the function of an orthomode transducer (OMT).

The interleaved subarray of below-cutoff apertures proposed (see Fig. 1) is a particular multiplexer case in which each aperture is fed by an evanescent-mode ridge-waveguide filter. The passband of each aperture is given by the passband of the feeding filter, whereas the polarization of the apertures is given by the orientation of the ridges in the filter.

A total of two filters must be designed to form the unit cell, as described in Section II. As a design example, we use in this paper two bands centered at 9.625 GHz and 10.375 GHz, with a bandwidth of 250 MHz and a minimum return loss level of 15 dB in the passband (the design goal will be 20 dB to provide margin against manufacturing tolerances). The designed rejection of each filter over the central frequency of the adjacent channel must be above 15 dB. These specifications, a down-scaled frequency version of the two channels considered in Ka-band multiple-beam applications, either for downlink (around 20 GHz) or uplink (around 30 GHz), can be satisfied (as a simplified proof-of-concept) with an in-line filter of order 2 with optimal equiripple response. In an up-scaled final application, channels would be closer. In particular, only 500 MHz are dedicated for users either for downlink or uplink [2] and, therefore, channels of no more than 200 MHz separated 50 MHz should be implemented. In this scenario, higher-order filter should be designed to increase the selectivity, thereby permitting a smaller separation between channels. It is worth mentioning that this separation is independent of the generation of grating lobes, which only depends on the electrical spacing (p/λ) between apertures.

Figure 6 shows the longitudinal configuration of the evanescent-mode ridge-waveguide filter. As can be observed, the resonators are conventional single-ridge waveguides connected through square waveguides working as inverters. A last waveguide section (with length L_3) is used to couple the energy from the last resonator to the free-space region. The length of the last section of below-cutoff waveguide (the last inverter) determines the coupling to the free-space region.

In this case, the filters are fed by a coaxial waveguide located at a height h_c from the bottom wall of the square waveguide housing. The inner conductor of the coaxial waveguide is introduced into the filter to excite the first resonator. The dimensions and materials of the feeding coaxial waveguide section are: $h_c = 6.05$ mm, $L_c = 5.00$ mm, $d_c = 1.27$ mm, $d_d = 4.10$ mm, and $\varepsilon_r = 2.10$. The relative position of the coaxial waveguide with respect to the waveguide walls must be always preserved, regardless of the orientation of the filter. Figure 7 illustrates the rotation of each filer to have two different polarization for each passband. Labels F9 and F10 refer to filters centered at 9.625 GHz and 10.375 GHz, respectively, and V/H to the polarization of the aperture.

The filters have been designed using the technique described in Section III (note that this technique is also valid for a

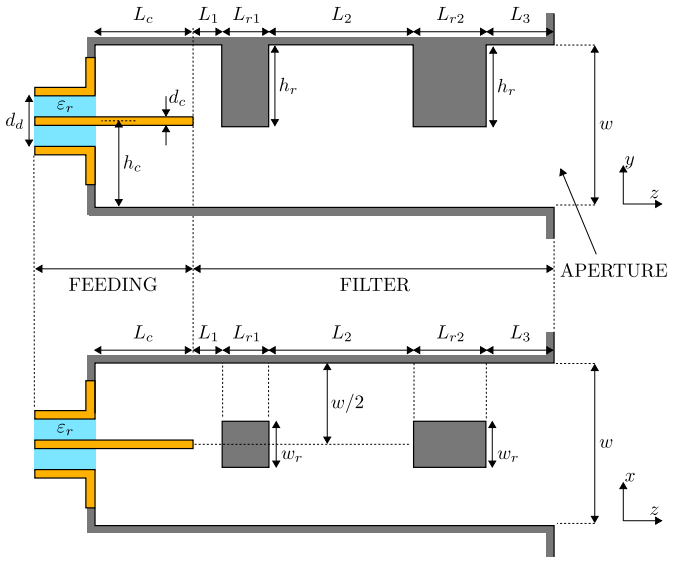

Figure 6. Longitudinal configuration of the open-ended evanescent-mode ridge-waveguide filters.

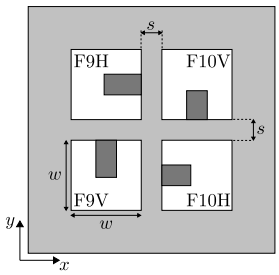

Figure 7. Distribution of apertures in the multiplexer.

Table II
DIMENSIONS (in mm) OF THE OPTIMIZED FILTERS

Parameter	Filter at 9.625 GHz	Filter at 10.375 GHz
L_1	1.65	1.95
L_{r1}	5.86	5.45
L_2	7.91	8.71
L_{r2}	3.72	3.66
L_3	1.78	2.46
h_r	5.00	4.50
w_r	3.50	3.50

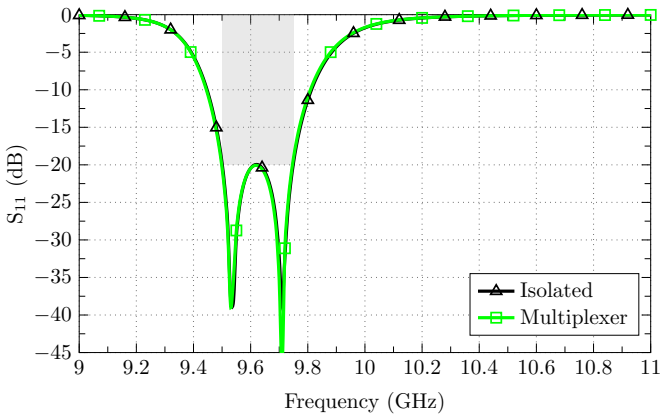

Figure 8. S_{11} parameter of the filter centered at 9.625 GHz optimized individually.

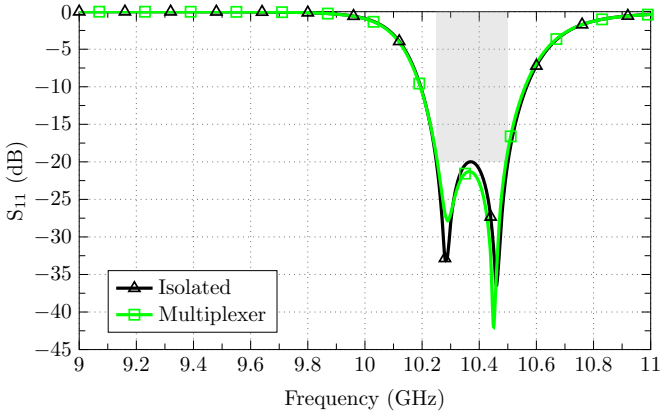

Figure 9. S_{11} parameter of the filter centered at 10.375 GHz optimized individually.

Table III
DIMENSIONS (in mm) OF THE OPTIMIZED FILTERS IN THE UNIT CELL

Parameter	F9V	F9H	F10V	F10H
L_1	1.65	1.65	1.95	1.95
L_{r1}	5.85	5.86	5.45	5.45
L_2	7.91	7.92	8.74	8.73
L_{r2}	3.67	3.68	3.71	3.71
L_3	1.78	1.80	2.59	2.59

coaxial feeding). Table II shows the final parameters for the two filters. It is important to note that, in order to facilitate the manufacturing process, the same height has been considered for all ridge resonators within each filter. As a result, only the lengths of the different resonators and inverters have been adjusted to achieve the desired response. This choice facilitates also the full wave EM analysis of the structure, since only one discontinuity needs to be analyzed to simulate rigorously all resonators.

Once the isolated filters are successfully designed, the unit cell of the multiplexer can be constructed according to the configuration shown in Fig. 7 by properly rotating the filters. Figs. 8 and 9 show the response of the filters centered at 9.625 GHz and 10.375 GHz, respectively, for two cases. The first case shows the response of each isolated filter. The second case shows the filters assembled to form the unit cell that is simulated as a whole (for simplicity, only the response for the vertically-polarized filters is shown). As can be observed, the lower-band filter is barely affected by the presence of the other filters, however, the filters centered at 10.375 GHz are affected by the other filters, even though the configuration shown in Fig. 7 minimizes the mutual coupling between apertures. To solve this problem, the filters of the unit cell must be optimized all together using the previous design as starting point and following the classic design procedure for multiplexers [34], namely, acting on a filter by filter basis and modifying first the filter dimensions closer to the manifold (in this case, the free-space). The final resulting dimensions are given in Table III.

The optimized unit cell can be replicated to form four inter-

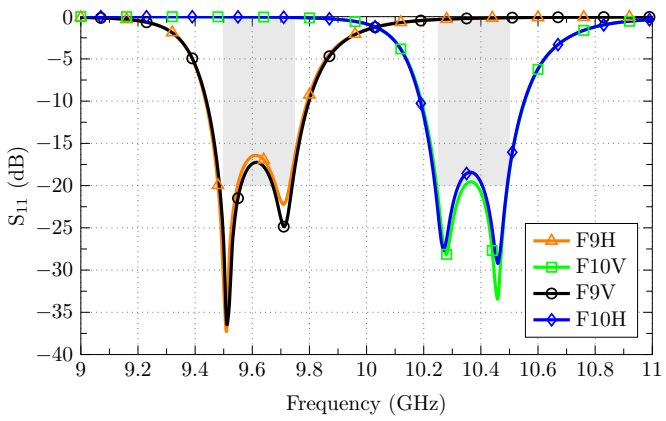

Figure 10. S_{11} parameter of the central unit cell of a 3×3 array of apertures with a period p =22.16 mm (0.8λ).

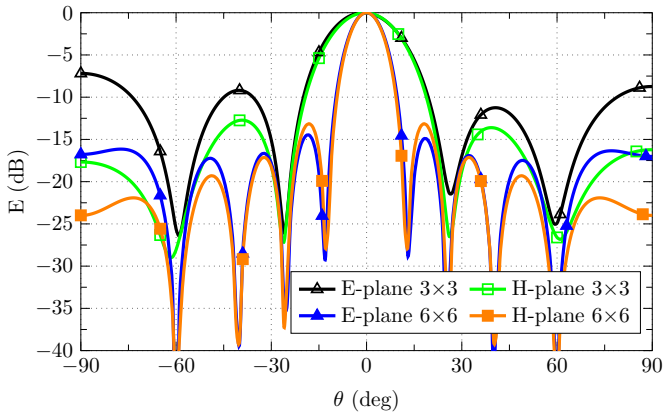

Figure 11. Radiation pattern of two arrays (3×3 and 6×6) of apertures at 10.375 GHz with a period p =22.16 mm (0.8λ).

leaved subarrays of below-cutoff apertures. Fig. 10 shows the S_{11} parameter of the central unit cell of the 3×3 configuration that is shown in Fig. 1 (b). As it can be observed, the filters are correctly centered within the desired passbands. Only the return loss level is affected by the presence of the surrounding cells, but it is still above the desired 15 dB level.

Fig. 11 shows the radiation pattern of the subarray with vertical polarization, and a passband centered at 10.375 GHz (F10V in Fig. 7). Two different configurations are considered in this case, namely a 3×3 array and a 6×6 array. These results illustrate the absence of higher-order grating lobes in the radiation pattern due to the small separation between apertures (p=0.8λ). The aperture efficiency in both cases is above 94%.

Alternative configurations to the one shown in Fig. 1 (b) can be envisaged. For instance, the array may be split into two arrays operating in two different bands, e.g. one centered at 9.625 GHz and the other one at 10.375 GHz. This configuration would reduce the periodicity in one direction half, and would also reduce the complexity of the BFN. However, the same periodicity as in Fig. 1 (b) should be kept in the orthogonal direction to interleave apertures with orthogonal polarizations (see unit cell for separate arrays in Table IV), which would produce a non-symmetric radiation pattern. In addition, the advantage of having interleaved sub-arrays to generate all downlink or uplink colors with a single structure would be lost. For instance, a precise alignment between the two arrays would be necessary to produce contiguous spot beams on Earth. Also, note that, in case of using the proposed interleaved subarrays to illuminate a reflector, as in a classical MBA solution, the interleaving would permit the overlapping of beam's footprints at the focus of a single reflector to produce contiguous spot beams on Earth. By having two separated structures, two different reflectors and two different feeding mechanisms would be necessary, thereby increasing the volume of the system with respect to the proposed interleaved solution.

Table IV
COMPARATIVE OF ALTERNATIVE CONFIGURATIONS

	Interleaved	Separate arrays	Wideband
Unit cell	F1H F2V / F1V F2H	Unit cell 1: F1V F1H; Unit cell 2: F2H F2V	V H
Number of arrays	1	2	1
Feeding network	Medium	Easy	Very complex

To keep all the array in a single structure, dual-band filters or wideband filters (allowing the pass of both frequencies) could be used. Under this configuration, the interleaving property is not lost, and all four downlink or uplink colors can be generated by a single structure. An advantage of this configuration is that a wider area of the array can be illuminated for each color, thus improving the aperture efficiency. The main drawback of this configuration lies in the feeding network, which must have a wider bandwidth of operation, and must include several diplexers to assign to each aperture the appropriate combination of signals. The complexity and cost of the feeding network is thus highly increased, compared to the proposed interleaved solution. This type of configuration is feasible, but, due to the complexity of the feeding network, only for a limited number of spots. Table IV shows a comparative of the alternative configurations.

V. PROTOTYPE AND MEASUREMENTS

The four-aperture radiator described in previous section has been fabricated in aluminum using CNC machining in order to validate our design procedure. Fig. 12 (a) shows a picture of the prototype ending in the radiating apertures. As we can see, the ridges are placed according to the configuration shown in Fig. 7. In order to minimize the manufacturing errors in the height of the ridges, the breadboard has been divided into three parts: two for the filter resonators, and one for the feeding connectors, as shown in Fig. 12 (b). These connectors are rotated 90° with respect to each other to guarantee the spacing between apertures in this breadboard. Note that this

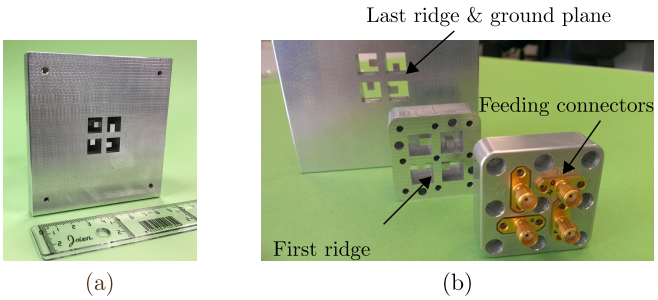

Figure 12. Fabricated breadboard formed by four apertures fed by four evanescent-mode single ridge-waveguide filters: (a) Front view of the complete structure (apertures on the ground plane), and (b) parts in which the breadboard has been cut to simplify manufacturing.

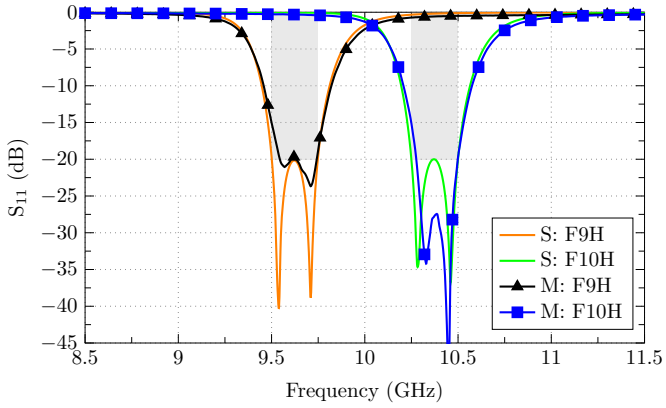

Figure 13. Measured (M) and simulated (S) S_{11} parameter of the horizontally-polarized elements of the fabricated breadboard.

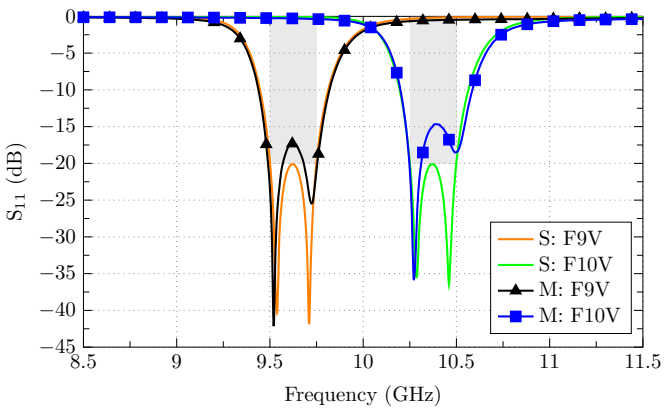

Figure 14. Measured (M) and simulated (S) S_{11} parameter of the vertically-polarized elements of the fabricated breadboard.

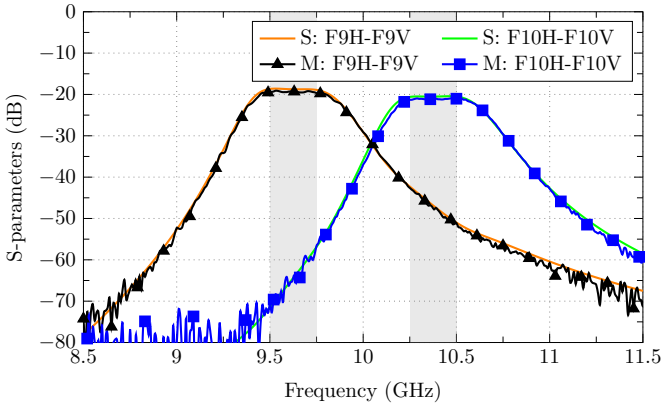

Figure 15. Measured (M) and simulated (S) mutual coupling (S_{21} parameter) between orthogonal elements centered at the same frequency.

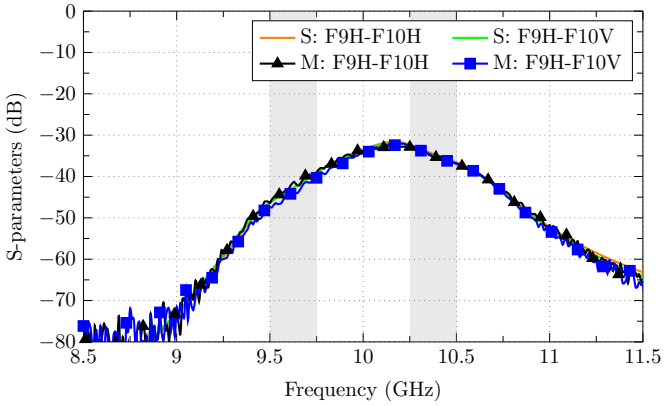

Figure 16. Measured (M) and simulated (S) mutual coupling (S_{21} parameter) between elements centered at the different frequencies.

breadboard represents the unit cell of the four interleaved subarrays shown in Fig. 1. Each subarray would be fed by an independent feeding network, with a single connector per subarray. Therefore, the connectors in the final structure would be placed further away and, thereby, a rotation of connectors would not be necessary, no matter the operational frequency band.

Figures 13 and 14 show the simulated and measured S_{11} parameter at the input port of each filter. In all cases, the measured response is centered around the pass band of each filter (indicated by shadowed regions) with a return loss level better than 15 dB. The discrepancies between measured and simulated results can be attributed to manufacturing tolerances. Alternatively, additive manufacturing techniques can be considered to avoid assembling problems [35].

The mutual coupling between the different elements of the breadboard, plotted in Figs. 15 and 16, indicates that the interaction between filters centered at different frequencies is quite low, below -32 dB within the two bands under study. However, the coupling between orthogonal elements operating at the same frequency is around -20 dB within the pass band of the filter. In order to decrease this coupling, alternative filter configurations can be considered.

The radiation pattern of the different elements has been measured at the central frequency in each band. Figs. 17 and 18 show the directivity of elements F9H and F10V [see Fig. 7] on the main planes. As can be observed, in both cases, the measured and simulated patterns are quite similar for both copolar and crosspolar components. Note that the shape of the patterns follows that of a small aperture since, in each case, only one aperture is being fed. The discrepancies between measured and simulated results around $\theta = 90°$ are caused by the assumption of an infinite ground plane in the simulations.

Feeding the radiating apertures through an evanescent-mode

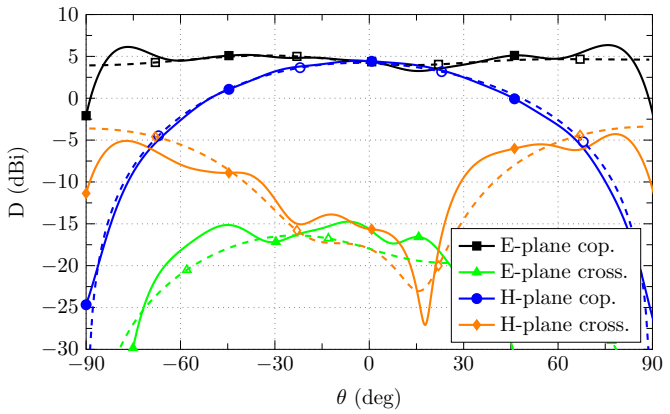

Figure 17. Measured (solid lines) and simulated (dashed lines) directivity on main planes of the element F9H at 9.625 GHz.

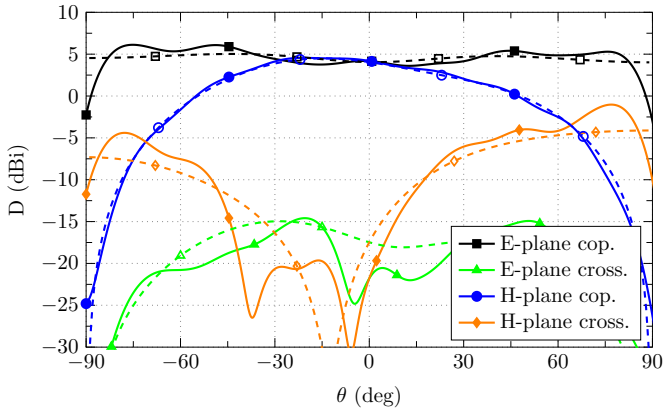

Figure 18. Measured (solid lines) and simulated (dashed lines) directivity on main planes of the element F10V at 10.375 GHz.

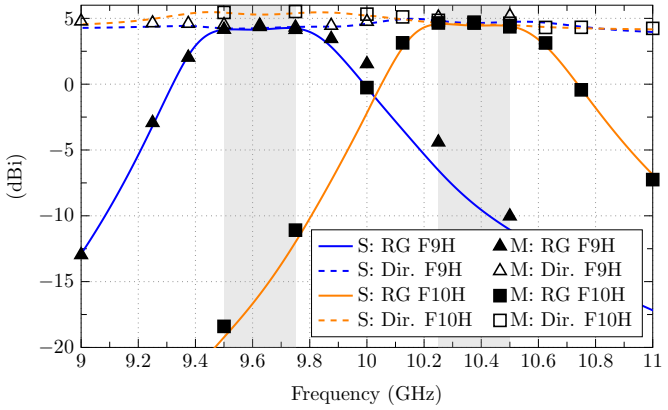

Figure 19. Measured (M) and simulated (S) directivity and realized gain at broadside of horizontally-polarized elements.

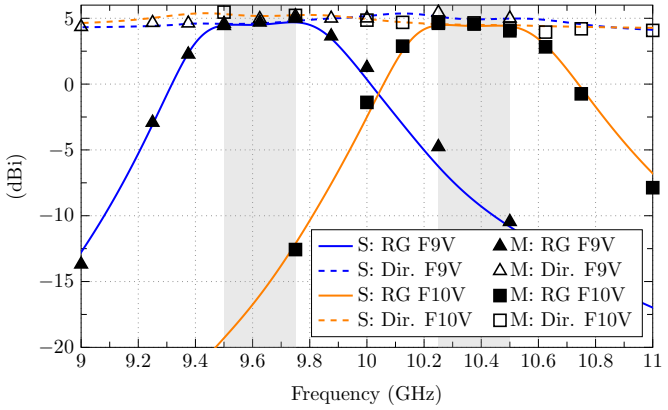

Figure 20. Measured (M) and simulated (S) directivity and realized gain (RG) at broadside of vertically-polarized elements.

ridge-waveguide filter makes the operating bandwidth of the apertures equal to the pass-band of the filter. To prove this behavior, Figs. 19 and 20 compare the simulated and measured realized gain and directivity at broadside for each element as a function of frequency. As we can see, the realized gain only approaches the directivity within the pass band of each filter, indicated by shadowed regions. Outside of these regions, the realized gain decays considerably and the filter no longer radiates. A more abrupt drop (or selectivity) of the realized gain outside the pass bands can be obtained using higher-order filters.

Finally, the use of evanescent-mode filters instead of larger above-cutoff rectangular waveguide filters (in order to reduce the size of the unit cell and avoid harmful grating lobes) will have an impact in terms of insertion losses and power-handling capabilities. The design reported in this paper has been carried out to obtain the larger dimensions for the apertures, and therefore for the filter housing (working essentially at the limit of 0.8λ of separation between apertures of the same color). As a result, the gap of the filters below the ridges is kept high for the frequency band of operation ($>$ 5 mm at 10 GHz), thus limiting the performance degradation. The measured insertion losses are below 0.4 dB in the passband (obtaining a radiation efficiency above 92%, including connectors), which is a good figure for filters manufactured in bare aluminum with coaxial excitation. Regarding power-handling capability, simulations performed with SPARK3D (from Aurorasat, now with Dassault Systèmes) of both isolated evanescent-mode filters suggests a multipactor continuous wave (CW) breakdown above 10 kW for the worst filter at the worst edge of the passband (and about 20 kW CW at the center frequency). Therefore, the critical point will be the coaxial connector used for exciting the filter (a standard SMA connector withstands around 50 W at 10 GHz). To increase the power-handling capability, high-power TNC or N coaxial connectors are required, whereas for higher power levels (i.e., $>$ 300 W CW), the filters must be excited by an above-cutoff ridge waveguide coming from an all-metallic BFN.

VI. Conclusion

In this paper we describe a new family of radiators consisting of four interleaved subarrays of square apertures. The unit cell of the radiator is formed by four apertures arranged in a 2×2 configuration. In order to avoid the appearance of grating lobes in the radiation pattern of each subarray, the lateral size of the unit cell is kept smaller than 0.8λ, and, therefore, the apertures are below cutoff.

The feeding of the below cutoff radiating apertures is achieved through evanescent-mode ridge-waveguide filters,

which also define the operating frequency band and polarization. A new design technique for in-line filters has been proposed, which is also suitable for filtering antennas. The new design technique provides an excellent structure without optimization. The individual filters are then assembled to form the complete radiator. The final dimensions are easily obtained with a fast global refinement of all radiating apertures so that all mutual coupling effects are taken into account.

In addition to theory, a prototype has also been fabricated and measured. Measured results show very good agreement with simulations. In particular, a return loss level better than 15 dB within the desired bands, and a mutual coupling between the different elements better than -20 dB have been achieved in all cases. The realized gain for each element confirms that the apertures only radiate within the pass band of each filter, with a realized gain around 5 dBi at broadside, and a total efficiency near 100% within the pass band of the radiating elements.

Although the family of radiators proposed in this paper is specifically intended for space applications, their use can be envisaged in all applications requiring multiple beam antennas. Furthermore, the input feeding can also be effectively implemented with ridge waveguides thereby further extending the range of possible applications.

For DRA applications, a phase shifter can be inserted at the input port of each filter, or at the input port of the feeding network of a group of elements, to provide the desired beam pointing. The insertion of these devices is independent of the design of the evanescent-mode ridge-waveguide filters. Additionally, a circularly-polarized radiation pattern can be obtained by using a polarizer in front of the apertures, e.g. a quad-ridge waveguide with 90°-phase-shifted fundamental modes, a fully metallic 3-D polarizer built from a below cutoff rectangular waveguide [36], or a feeding network providing the proper relative phases to each individual radiator.

Finally, the same basic concept can also be implemented using stacked PCB technology. In conclusion, we do believe that the new family of radiators that we describe in this paper can indeed become an enabling technology for both space and ground multiple beam antenna systems.

REFERENCES

[1] P. Angeletti, F. Coromina, F. Deborgies, R. De Gaudenzi, A. Ginesi, and A. Vernucci, "Satcoms 2020 R&D challenges: Part I: Broadband fixed communications," in *27th IET and AIAA International Communications Satellite Systems Conference (ICSSC)*, 2009.

[2] H. Fenech, S. Amos, A. Tomatis, and V. Soumpholphakdy, "High throughput satellite systems: An analytical approach," *IEEE Transactions on Aerospace and Electronic Systems*, vol. 51, no. 1, pp. 192–202, 2015.

[3] S. K. Rao, "Advanced antenna technologies for satellite communications payloads," *IEEE Trans. Antennas Propag.*, vol. 63, no. 4, pp. 1205–1217, 2015.

[4] M. Schneider, C. Hartwanger, and H. Wolf, "Antennas for multiple spot beam satellites," *CEAS Space Journal*, vol. 2, no. 1-4, pp. 59–66, 2011.

[5] E. Amyotte, Y. Demers, L. Hildebrand, M. Forest, S. Riendeau, S. Sierra-Garcia, and J. Uher, "Recent developments in Ka-band satellite antennas for broadband communications," in *4th European Conference on Antennas and Propagation (EuCAP)*. IEEE, 2010.

[6] G. Doro, F. De Gennaro, M. Lisi, and A. Roederer, "Beam forming network for a multibeam antenna at 20 GHz," in *14th European Microwave Conference*. IEEE, 1984, pp. 691–696.

[7] M. Schneider, C. Hartwanger, E. Sommer, and H. Wolf, "The multiple spot beam antenna project "medusa"," in *3rd European Conference on Antennas and Propagation (EuCAP)*. IEEE, 2009, pp. 726–729.

[8] C. Leclerc, M. Romier, H. Aubert, and A. Annabi, "Ka-band multiple feed per beam focal array using interleaved couplers," *IEEE Transactions on Microwave Theory and Techniques*, vol. 62, no. 6, pp. 1322–1329, 2014.

[9] J. M. Montero, A. M. Ocampo, and N. J. Fonseca, "C-band multiple beam antennas for communication satellites," *IEEE Trans. Antennas Propag.*, vol. 63, no. 4, pp. 1263–1275, 2015.

[10] H. Chreim, R. Chantalat, M. Thévenot, U. Naeem, S. Bila, T. Monédière, B. Palacin, Y. Cailloce, G. Caille, and P. De Maagt, "An enhanced Ka-band reflector focal-plane array using a multifeed EBG structure," *IEEE Antennas and Wireless Propagation Letters*, vol. 9, pp. 1152–1156, 2010.

[11] G. Caille, R. Chiniard, M. Thevenot, H. Chreim, E. Arnaud, T. Monediere, P. de Maagt, and B. Palacin, "Electro-magnetic band-gap feed overlapping apertures for multi-beam antennas on communication satellites," in *8th European Conference on Antennas and Propagation (EuCAP)*. IEEE, 2014, pp. 963–967.

[12] G. Toso, P. Angeletti, and C. Mangenot, "Multibeam antennas based on phased arrays: An overview on recent ESA developments," in *8th European Conference on Antennas and Propagation (EuCAP)*. IEEE, 2014, pp. 178–181.

[13] D. Petrolati, P. Angeletti, and G. Toso, "A lossless beam-forming network for linear arrays based on overlapped sub-arrays," *IEEE Trans. Antennas Propag.*, vol. 62, no. 4, pp. 1769–1778, 2014.

[14] Y. V. Krivosheev, A. V. Shishlov, and V. V. Denisenko, "Grating lobe suppression in aperiodic phased array antennas composed of periodic subarrays with large element spacing," *IEEE Antennas and Propagation Magazine*, vol. 57, no. 1, pp. 76–85, 2015.

[15] T. Suda, T. Takano, and Y. Kazama, "Grating lobe suppression in an array antenna with element spacing greater than a half wavelength," in *IEEE Antennas and Propagation Society International Symposium (APSURSI)*, 2010, pp. 1–4.

[16] P. Angeletti, G. Toso, and G. Ruggerini, "Array antennas with jointly optimized elements positions and dimensions part II: Planar circular arrays," *IEEE Trans. Antennas Propag.*, vol. 62, no. 4, pp. 1627–1639, 2014.

[17] A. I. Sandhu, E. Arnieri, G. Amendola, L. Boccia, E. Meniconi, and V. Ziegler, "Radiating elements for shared aperture Tx/Rx phased arrays at K/Ka band," *IEEE Trans. Antennas Propag.*, vol. 64, no. 6, pp. 2270–2282, 2016.

[18] C.-X. Mao, S. Gao, Q. Luo, T. Rommel, and Q.-X. Chu, "Low-cost X/Ku/Ka-band dual-polarized array with shared aperture," *IEEE Trans. Antennas Propag.*, vol. 65, no. 7, pp. 3520–3527, 2017.

[19] V. E. Boria Esbert, M. Baquero Escudero, M. Guglielmi, P. Angeletti, and G. Toso, "Celda radiante para antena multihaz," *Spanish Patent ES 2647279B2*, Jun 2017.

[20] Y. Yusuf and X. Gong, "Compact low-loss integration of high-Q 3-D filters with highly efficient antennas," *IEEE Transactions on Microwave Theory and Techniques*, vol. 59, no. 4, pp. 857–865, 2011.

[21] H. Chu, J.-X. Chen, S. Luo, and Y.-X. Guo, "A millimeter-wave filtering monopulse antenna array based on substrate integrated waveguide technology," *IEEE Trans. Antennas Propag.*, vol. 64, no. 1, pp. 316–321, 2016.

[22] I. Wolff, C. Günner, J. Kassner, R. Kulke, and P. Uhlig, "New heights for satellites: LTCC multilayer technology for future satellites," *IEEE Microwave Magazine*, vol. 19, no. 1, pp. 36–47, Jan 2018.

[23] C. X. Mao, S. Gao, Y. Wang, B. Sanz-Izquierdo, Z. Wang, F. Qin, Q. X. Chu, J. Li, G. Wei, and J. Xu, "Dual-band patch antenna with filtering performance and harmonic suppression," *IEEE Trans. Antennas Propag.*, vol. 64, no. 9, pp. 4074–4077, 2016.

[24] C.-K. Lin and S.-J. Chung, "A filtering microstrip antenna array," *IEEE Transactions on Microwave Theory and Techniques*, vol. 59, no. 11, pp. 2856–2863, 2011.

[25] F.-C. Chen, J.-F. Chen, Q.-X. Chu, and M. J. Lancaster, "X-band waveguide filtering antenna array with nonuniform feed structure," *IEEE Transactions on Microwave Theory and Techniques*, vol. 65, no. 12, pp. 4843–4850, 2017.

[26] P. Ludlow, V. Fusco, G. Goussetis, and D. E. Zelenchuk, "Applying band-pass filter techniques to the design of small-aperture evanescent-mode waveguide antennas," *IEEE Trans. Antennas Propag.*, vol. 61, no. 1, pp. 134–142, 2013.

[27] M. Guglielmi, "Simple CAD procedure for microwave filters and multiplexers," *IEEE Transactions on Microwave Theory and Techniques*, vol. 42, no. 7, pp. 1347–1352, 1994.

[28] P. Soto, D. De Llanos, E. Tarín, V. Boria, B. Gimeno, A. Onoro, I. Hidalgo, and J. Padilla, "Efficient analysis and design strategies for evanescent mode ridge waveguide filters," in *36th European Microwave Conference*, 2006, pp. 1095–1098.
[29] D. Sánchez-Escuderos, M. Baquero-Escudero, P. Soto, V. E. Boria, and M. Guglielmi, "On multimode equivalent network representation of finite arrays of open-ended waveguides," *IEEE Trans. Antennas Propag.*, vol. 65, no. 8, pp. 4334–4339, 2017.
[30] G. F. Craven and C. K. Mok, "The design of evanescent mode waveguide bandpass filters for a prescribed insertion loss characteristic," *IEEE Transactions on Microwave Theory and Techniques*, vol. 19, no. 3, pp. 295–308, 1971.
[31] R. J. Cameron, C. M. Kudsia, and R. R. Mansour, *Microwave Filters for Communication Systems: Fundamentals, Design, and Applications*. John Wiley & Sons, 2018.
[32] G. F. Craven and R. F. Skedd, *Evanescent mode microwave components*. Artech House, 1987.
[33] H. Y. Hwang and S.-W. Yun, "The design of bandpass filters considering frequency dependence of inverters," *Microwave Journal*, vol. 45, no. 9, pp. 154–163, 2002.
[34] R. J. Cameron and M. Yu, "Design of manifold-coupled multiplexers," *IEEE Microwave Magazine*, vol. 8, no. 5, pp. 46–59, 2007.
[35] J. S. Silva, M. Garcia-Vigueras, T. Debogović, J. R. Costa, C. A. Fernandes, and J. R. Mosig, "Stereolithography-based antennas for satellite communications in ka-band," *Proceedings of the IEEE*, vol. 105, no. 4, pp. 655–667, 2017.
[36] C. Molero and M. García-Vigueras, "Circuit modeling of 3-D cells to design versatile full-metal polarizers," *IEEE Transactions on Microwave Theory and Techniques*, 2019.

Daniel Sánchez-Escuderos (S'05-M'09) was born in Vila-real, Spain, on October 20, 1980. He received the Telecommunications Engineering degree and the Ph.D. degree from the Universitat Politècnica de València (UPV), Valencia, Spain, in 2004 and 2009, respectively.

Since 2005, he has been with the Institute of Telecommunications and Multimedia Applications of the UPV. In 2009, he was hired as a Post-Doctoral Researcher under the framework of several research activities. From 2009 to 2014 he was involved in a national research project in terahertz technology. Since 2014, he has collaborated in several European projects supported by the European Space Agency and, also, in national research projects. His main research interests include antenna measurements, frequency-selective surface (FSS) structures, millimeter and submillimeter-wave technology, gap-waveguide technology, and microwave filters.

Dr. Sánchez-Escuderos has been session chair at several scientific conferences, and has been a member of the IEEE Antennas and Propagation Society (IEEE AP-S) since 2005. He was the recipient of an FPI National Scholarship in support of his doctorate studies (2005).

Jesús Ruiz Garnica was born in Tarragona, Spain, in 1986. He received the B.S. degree in telecommunication engineering and M.S. degree in communication systems, technologies and networks from the Universidad Politècnica de València, Valencia, Spain, in 2012 and 2014, respectively, where he is currently pursuing the Ph.D. degree.

In 2014, he was a trainee with the Val Space Consortium, Valencia, where he was involved in the design of microwave passive devices for high power applications in satellite communications. In 2015, he was a Researcher with the Instituto de Telecomunicaciones y Aplicaciones Multimedia, Universidad Politècnica de València. His current research interests include the design of novel passive waveguide components.

Mariano Baquero-Escudero (S'87-M'90) was born in Murcia, Spain, on January 11, 1962. He received the degree in telecommunications engineering from the Polytechnic University of Catalonia (UPC), Barcelona, Spain, in 1986 and the Ph.D. degree from the Polytechnic University of Valencia (UPV), Valencia, Spain, in 1994. He became a Member (M) of IEEE in 1987.

He was with the Antennas, Microwave and Radar Group, UPC, from 1986 to 1988, where he worked on the development of a cylindrical near-field facility to measure a 3-D radar antenna in CESELSA. Since 1989, he has been with the UPV where he became a Full Professor in 2003. During 1995, he held a postdoctoral grant at the Joint Research Centre, European Commission, Ispra, Italy, where he developed high-resolution algorithms for radar applications. From April 1996 to February 1998, he was a Vice-Dean of the Telecommunications Engineering School of Valencia. He is currently with the Communications Department and into the Institute of Telecommunications and Multimedia Application of the Polytechnic University of Valencia. His main research interests include microwave circuit and antenna analysis, design and measurement.

Pablo Soto (S'01-M'06) was born in 1975 in Cartagena, Spain. He received the M.S. degree and Ph.D. degree (cum Laude) in Telecommunication Engineering from the Universidad Politecnica de Valencia in 1999 and 2012, respectively.

In 2000, he joined the Departamento de Comunicaciones, Universidad Politécnica de Valencia, where he is Associate Professor since 2012. He was an EU research fellow with the European Space Research and Technology Centre (ESTEC-ESA), Noordwijk, the Netherlands in 2000. His research interests comprise numerical methods for the analysis, synthesis, and fully automated design of passive components in waveguide and planar technologies, the development and design of novel hardware for satellite applications, and high-power RF effects.

Dr. Soto received the 2000 and 2012 COIT/AEIT national awards to the best Master Thesis and best Ph.D Thesis, respectively. He is also the co-recipient of the 2013 Gheorghe Cartianu Award of the Acadamia Romana.

Vicente E. Boria (S'91-A'99-SM'02-F'18) was born in Valencia, Spain, on May 18, 1970. He received his "Ingeniero de Telecomunicación" degree (with first-class honors) and the "Doctor Ingeniero de Telecomunicación" degree from the Universidad Politécnica de Valencia, Valencia, Spain, in 1993 and 1997, respectively.

In 1993 he joined the "Departamento de Comunicaciones", Universidad Politécnica de Valencia, where he has been Full Professor since 2003. In 1995 and 1996, he was holding a Spanish Trainee position with the European Space Research and Technology Centre, European Space Agency (ESTEC-ESA), Noordwijk, The Netherlands, where he was involved in the area of EM analysis and design of passive waveguide devices. He has authored or co-authored 10 chapters in technical textbooks, 180 papers in refereed international technical journals, and over 200 papers in international conference proceedings. His current research interests are focused on the analysis and automated design of passive components, left-handed and periodic structures, as well as on the simulation and measurement of power effects in passive waveguide systems.

Dr. Boria has been a member of the IEEE Microwave Theory and Techniques Society (IEEE MTT-S) and the IEEE Antennas and Propagation Society (IEEE AP-S) since 1992. He is also member of the European Microwave Association (EuMA), and has been the Chair of the 48th European Microwave Conference held in Madrid, Spain. He acts as a regular reviewer of the most relevant IEEE and IET technical journals on his areas of interest. He has been Associate Editor of IEEE Microwave and Wireless Components Letters (2013-2018) and IET Electronics Letters (2015-2018). Presently, he serves as Subject Editor (Microwaves) of IET Electronics Letters, and as Editorial Board member of International Journal of RF and Microwave Computer-Aided Engineering. He is also member of the Technical Committees of the IEEE-MTT International Microwave Symposium and of the European Microwave Conference.

Giovanni Toso (IEEE S'1993, M'00, SM '07) received the Laurea Degree (cum laude), the Ph.D. and the Post Doctoral Fellowship from the University of Florence, Italy, in 1992, 1995 and 1999.

In 1996 he was visiting scientist at the Laboratoire d'Optique Electromagnétique, Marseille (France). In 1999 he was a visiting scientist at the University of California (UCLA) in Los Angeles, he received a scholarship from Alenia Spazio (Rome, Italy) and he has been appointed researcher in a Radio Astronomy Observatory of the Italian National Council of Researches (CNR). Since 2000 he is with the Antenna and Submillimeter Waves Section of the European Space Agency, ESA ESTEC, Noordwijk, The Netherlands. He has been initiating and contributing to several R&D activities on satellite antennas based on arrays, reflectarrays, discrete lenses and reflectors. In particular, in the field of onboard satellite antennas, he has been coordinating activities on multibeam antennas (active and passive) mainly for Telecom Applications. In the field of terminal antennas for Telecom applications, he has been initiating several R&D activities on reconfigurable antennas with electronic and mechanical scanning.

G. Toso has been coauthoring the best paper at the 30th ESA Antenna Workshop and the most innovative paper at the 30th and 36th ESA Antenna Workshops. He holds about 20 international patents. In 2009 he has been coeditor of the Special Issue on Active Antennas for Satellite Applications in the International Journal of Antennas and Propagation. In 2014 he has been guest editor, together with Dr. R. Mailloux, of the Special Issue on "Innovative Phased array antennas based on non-regular lattices and overlapped subarrays" published in the IEEE Transactions on Antennas and Propagation and, for the same society, has been an Associate Editor (2013-2016). Since the first edition in 2006 he has been significantly contributing to the ESoA course on Satellite Antennas. Since 2010, together with Dr. P. Angeletti, he has been instructing short courses on Multibeam Antennas and Beamforming Networks during international conferences (IEEE APS, IEEE IMS, IEEE IWCS, EUCAP, EuMW) that have been attended by more than 600 participants. Giovanni has been the chairman of the 39th ESA Antenna Workshop on "Multibeam and Reconfigurable Antennas". In 2018 G. Toso received, together with Prof. A. Skrivervik, the Best Teacher Award of the European School of Antennas (ESoA)

Piero Angeletti (EuMA member) received the Laurea degree in Electronics Engineering from the University of Ancona (Italy) in 1996, and the PhD in Electromagnetism from the University of Rome "La Sapienza" (Italy) in 2010.

His 18 years experience in RF Systems engineering and technical management encompasses conceptual/architectural design, trade-offs, detailed design, production, integration and testing of satellite payloads and active antenna systems for commercial/military telecommunications and navigation (spanning all the operating bands and set of applications) as well as for multifunction RADARs and electronic counter measure systems. Dr. Angeletti is currently member of the technical staff of the European Space Research and Technology Center (ESTEC) of the European Space Agency, in Noordwijk (The Netherlands). He is heading the Radio Frequency Payloads and Technology Division of the ESA Directorate of Technology, Engineering and Quality (TEC), which is responsible for RF payloads, instruments and relevant technologies. In particular he oversees ESA R&D activities related to flexible satellite payloads, RF front-ends and on-board digital processors.

Dr. Angeletti authored/co-authored over 200 technical reports, book chapters and papers published in peer reviewed professional journals and international conferences' proceedings.

Marco Guglielmi was born in Rome, Italy, on December 17, 1954. He received the degree "Laurea in Ingegneria Elettronica" in 1979 from the University of Rome "La Sapienza", Rome, Italy, where in 1980 he also attended the "Scuola di Specializzazione in Elettromagnetismo Applicato". In 1981 he was awarded a Fulbright Scholarship in Rome, Italy, and an HISP (Halsey International Scholarship Programme) from the University of Bridgeport, Bridgeport, Connecticut, USA, where in 1982 he obtained an MS Degree in Electrical Engineering. In 1986 he received a PhD degree in Electrophysics from the Polytechnic University, Brooklyn, New York, USA.

From 1984 to 1986 he was Academic Associate at Polytechnic University, and from 1986 to 1988 he was Assistant Professor in the same institution. From 1988 to 1989 he was Assistant Professor at the New Jersey Institute of Technology, Newark, New Jersey, USA. In 1989 he joined the European Space Agency as a Senior Microwave Engineer in the RF System Division of the European Space Research and Technology Centre (ESTEC), Noordwijk, The Netherlands, where he was in charge of the development of microwave filters and electromagnetic simulation tools. In 2001 he was appointed Head of the Technology Strategy Section of ESTEC where he contributed to the development of management processes and tools for the formulation of a European strategy for Space Technology Research and Development.

In 2014 Dr. Guglielmi retired from the European Space Agency and is currently holding the position of Invited Senior Researcher at the Polytechnic University of Valencia, Valencia, Spain. Dr. Guglielmi has been elevated to the grade of Fellow of the IEEE in January 2013 "For contributions to multimode equivalent networks and microwave filter design".